

# A Massive Jet Ejection Event from the Microquasar SS 433 Accompanying Rapid X-Ray Variability

T. Kotani<sup>1</sup>, S. A. Trushkin<sup>2</sup>, R. Valiullin<sup>3</sup>, K. Kinugasa<sup>4</sup>, S. Safi-Harb<sup>5</sup>, N. Kawai<sup>1</sup>, and M. Namiki<sup>6</sup>

kotani@hp.phys.titech.ac.jp

## ABSTRACT

Microquasars occasionally exhibit massive jet ejections which are distinct from the continuous or quasi-continuous weak jet ejections. Because those massive jet ejections are rare and short events, they have hardly been observed in X-ray so far. In this paper, the first X-ray observation of a massive jet ejection from the microquasar SS 433 with the Rossi X-ray Timing Explorer (RXTE) is reported. SS 433 undergoing a massive ejection event shows a variety of new phenomena including a QPO-like feature near 0.1 Hz, rapid time variability, and shot-like activities. The shot-like activity may be caused by the formation of a small plasma bullet. A massive jet may consist of thousands of those plasma bullets ejected from the binary system. The size, mass, internal energy, and kinetic energy of the bullets and the massive jet are estimated.

*Subject headings:* X-rays: individual (SS 433)

## 1. Introduction

Microquasars are stellar X-ray binaries (neutron stars or black holes) from which relativistic jets emanate via an unknown, very efficient mechanism (Mirabel & Rodríguez 1999).

---

<sup>1</sup>Tokyo Tech, 2-12-1 O-okayama, Tokyo 152-8551, Japan

<sup>2</sup>Special Astrophysical Observatory RAS, Nizhnij Arkhyz, Karachaevo-Cherkassia 369167, Russia

<sup>3</sup>Astrophysical Institute of Kazakh Academy of Sciences, 480020 Alma Ata, Kazakhstan

<sup>4</sup>Gunma Astronomical Observatory, 6860-86 Nakayama, Takayama, Agatsuma, Gunma 377-0702, Japan

<sup>5</sup>University of Manitoba, Winnipeg, Manitoba, Canada

<sup>6</sup>Osaka University, 1-1 Machikaneyama, Toyonaka, Osaka 560-0043, Japan

Microquasars such as SS 433 and GRS 1915+105 occasionally exhibit massive jet ejections, which are recognized as sporadic flares in their radio light curves (Fiedler et al. 1987; Foster et al. 1996). Because the massive jet ejections are rare (a few per year), short (within a few days), and aperiodic, pointing X-ray observations of these events have hardly been performed so far. As for SS 433, no X-ray observation has been confirmed to coincide with a radio flare, except for one or two possible coincident observations with Einstein in 1979 (Band 1989). A monitoring observation over 10 days and a long-look observation lasting 13 days were performed with ASCA in 1995 and 2000 (Kotani 1997; Namiki et al. 2001), but there was no radio flare coinciding the periods. A multi-wavelength observation with RXTE and the Giant Meter Radio Telescope in 2002 also misses radio flares (Chakrabarti et al. 2003). It should be stressed that the massive jets are distinct from the stable continuous jets of SS 433 and the quasi-continuous or weak jet of GRS 1915+105. The radio activity of SS 433 monitored with the Green Bank Interferometer over years may be characterized as a clustering of flare events separated by periods of quiescent emission (Fiedler et al. 1987). In those sporadic radio flare events, the radio flux density at 2.3 GHz exceeds 1 Jy, and massive jet blobs, which are recognized as bright extended spots in radio images, are ejected from the core of SS 433 at a quarter of the speed of light (Vermeulen et al. 1993). The ejection of massive jet blobs from GRS 1915+105 with a radio flux exceeding 100 mJy, by which the source has been recognized as a microquasar in the first place (Mirabel & Rodríguez 1994; Fender 2001), have been hardly observed in X rays (Muno et al. 2001), in contrast to a number of reports on the X-ray observation of the quasi-continuous or weak jet ejections (Mirabel et al. 1998; Klein-Wolt et al. 2002; Ueda et al. 2002).

We report on a successful X-ray observation of a massive jet ejection from SS 433 with the Rossi X-ray Timing Explorer (RXTE). The observation scheme is described in § 2, the data are analyzed and discussed in § 3.

## 2. Observations

Formerly, a radio flare was the only indicator of a massive jet ejection. Unfortunately, an X-ray observation triggered by a radio flare is too late to catch the moment of the ejection, as experienced in the cases of several previous target-of-opportunity (TOO) X-ray observations. Because the X-ray activity precedes a radio flare, a TOO X-ray observation will not work for a massive jet ejection event. So we have built a strategy to observe a *second* massive jet ejection event following the first event. In the active state of SS 433, radio flares are clustered with an interval of 8 – 23 days (Fiedler et al. 1987). Therefore, a series of monitoring observations triggered by a massive jet ejection may cover the moment

of a second ejection in 23 days.

We planned a 30-days-long TOO monitoring observation of SS 433 with RXTE to be triggered by a radio flare. The proposal was accepted in the Cycle 6 of the RXTE Guest Observer Program carried out for one year beginning in March 2001. The daily radio activity of the source has been monitored with the RATAN-600 radio telescope (Korolkov & Pariiskii 1979) of the Special Astrophysical observatory of the Russian Academy of Sciences (SAO RAS) since September 2001. After two months of static activity with an average flux density of 0.7 Jy at 2.3 GHz, a remarkable flare occurred on 2001 November 2 (MJD = 52215), indicating that the source entered its active state (Fig. 1). Flux densities reached 1.3 Jy at 2.3 GHz on MJD = 52216.6 (Kotani & Trushkin 2001; Trushkin et al. 2003). We started a series of X-ray observations with RXTE on MJD = 52222 (Kotani et al. 2003; Safi-Harb & Kotani 2003). Except for a break at MJD = 52231, SS 433 was observed for 3 ks every day. In the X-ray light curve, a temporal variation with time scales of 10 – 100 s appeared on MJD = 52225 and the amplitude increased day by day (Fig. 3). On MJD = 52232, the amplitude reached a maximum, and the 2-10 keV X-ray flux reached a local maximum of  $2.5 \times 10^{-10}$  erg s<sup>-1</sup> cm<sup>-2</sup>. The X-ray emission, thought to originate in the hot part of the jets as long as or longer than  $10^{12}$  cm, had never shown such a variability in past observations (Safi-Harb & Kotani 2003). Following the maximum of the flux and the variation amplitude, a second radio flare was detected on MJD = 52235. Due to a missing radio data point at MJD = 52234, the precise onset time and peak flux of the second flare are unfortunately not known, but they are not likely out of a range  $52233 < \text{MJD} \leq 52235$  and  $1.5 \text{ Jy} < F < 2 \text{ Jy}$ . Thus we conclude that the moment of a massive jet ejection was observed in the X-ray band. After the peak, the X-ray flux dropped due to a binary eclipse. The X-ray monitoring observation lasted until MJD = 52238, for 17 days, providing 16 data sets. An observation log is shown in Table 1. Optical spectroscopic observations were performed on MJD = 52220.6, 52221.6, and 52225.6 with the 0.7-m telescope at the observatory Kamenskoe Plato (Mironov & Tereshchenko 1998), and on MJD = 52229.39 and 52233.38 with the 0.65-m telescope at the Gunma Astronomical Observatory (Hasegawa et al. 2004; Kinugasa et al. 2002). Based on the spectroscopic data, the variation of the Doppler shifts of the jets during the campaign are estimated. The Doppler parameter of the receding jet is estimated to increase from 0.07 on MJD = 52222 to 0.13 on 52238, and that of the approaching jet decrease from  $-0.02$  to  $-0.07$ .

### 3. Data Analysis and Discussion

#### 3.1. The QPO-like feature

Firstly, we have searched for a periodicity in the data. No coherent pulsation has been detected from the 16 data sets, but a feature which can be interpreted as a QPO has been found at 0.1 Hz in the sum of the 16 power density spectra. The sum of the power density spectra is shown in Fig. 2. The fraction of the flux accounts for the QPO-like variation is estimated from the ratio of the Gaussian normalization to the area under the power-law continuum

This is the first detection of any periodicity or quasi periodicity shorter than 1 day from this source. Interestingly, other microquasars such as GRS 1915+105 also show 0.5-10 Hz low-frequency QPOs, which are considered to represent a characteristic time scale in the accretion flow (Muno et al. 2001). A super-critical accretion flow, which SS 433 is believed to have, had not been observed in the X-ray band because of the bright jets. The 0.1 Hz QPO-like feature may be the first detection of the super-critical accretion flow or disk in the X-ray band. The similarity to the QPO in other microquasars suggests the presence of a common mechanism working in other systems and SS 433, at least when the latter is undergoing a massive jet ejection.

#### 3.2. Spectral fitting

The sixteen data sets have been reduced with the standard reduction method<sup>1</sup>. The spectra are fitted with an empirical model,

$$e^{-\sigma(E)N_{\text{H}}} \times [\text{bremsstrahlung}(kT) + F_{\text{N}} \times \text{narrowline}(E_{\text{N}}, \sigma_{\text{N}}) + F_{\text{B}} \times \text{boradline}(E_{\text{B}}, \sigma_{\text{B}})], \quad (1)$$

where  $\sigma(E)$  is the absorption cross section,  $F_{\text{N}}$  and  $F_{\text{B}}$  are line fluxes,  $E_{\text{N}}$  and  $E_{\text{B}}$  are line center energies, and  $\sigma_{\text{N}}$  and  $\sigma_{\text{B}}$  are line widths. The hydrogen column density  $N_{\text{H}}$  and the width of the narrow line  $\sigma_{\text{N}}$  are fixed to  $6 \times 10^{21} \text{ cm}^{-2}$  and 0 keV, respectively. The results are shown in Table 2. The model has been applied to SS 433's spectra obtained with the LAC/Ginga (Kawai 1989; Yuan et al. 1995), a proportional counter array whose energy resolution and energy band are similar to those of the PCA. This model is a simple approximation of the complicated, line-abundant spectrum revealed with finer energy resolutions of SIS/ASCA (Kotani et al. 1996) and HETGS/Chandra (Marshall et al. 2002). In this model,

---

<sup>1</sup>RXTE GOF, [http://heasarc.gsfc.nasa.gov/docs/xte/xhp\\_proc\\_analysis.html](http://heasarc.gsfc.nasa.gov/docs/xte/xhp_proc_analysis.html)

the Doppler-shifted pairs of FeXXV  $K\alpha$ , FeXXVI  $K\alpha$ , and NiXXVII  $K\alpha$  lines are blended into the “narrow” and “broad iron lines.” The parameters which can not be determined from an RXTE spectrum, such as line flux ratios FeXXVI/Fe XXV and red/blue, are naturally eliminated from the model. The average spectrum of each data set and its evolution can be reproduced with the model and the spectral parameters in Table 2 together with the 2-10 keV fluxes in Fig. 1.

In the eclipse at MJD = 52234, both the bremsstrahlung temperature and the line fluxes drop, as observed with the LAC/Ginga (Kawai 1989; Yuan et al. 1995). The equivalent width of the two lines at the flux maximum (MJD = 52232) and the eclipse (MJD = 52234) are 1.76 keV and 1.56 keV, respectively. The equivalent width is not sensitive to eclipse because the base of the jet, which is responsible to both of the Doppler-shifted line emission and the continuum emission, is occulted in eclipse (Kawai 1989; Yuan et al. 1995; Gies et al. 2002).

### 3.3. The rapid variability

**Data analysis** Then we examined the rapid variation seen on MJD = 52232 (Fig. 3). The variation, which might appear irregular or chaotic, can be interpreted as a series of “shots” or “spikes” with widths of tens of seconds. Their intervals are random and do not show any periodicity. We have sampled 12 shots as indicated in Fig. 3, and folded the light curve to make the average profile of the shots (Fig. 4). The shot rises fast then slightly softens during the decay. The 8.4-21 keV profile is fitted with a burst model,

$$\text{const.} + A \times \begin{cases} 0 & (t \leq t_0) \\ \frac{t-t_0}{-t_0} & (t_0 \leq t \leq 0) \\ \exp(-t/\tau_{\text{dec}}) & (0 \leq t) \end{cases}, \quad (2)$$

where  $A$  is a normalization factor,  $t$  is the time from the peak,  $t_0$  is the time of the onset of the shot, and  $\tau_{\text{dec}}$  is the decay time scale. The onset time and decay time scale are fitted to be  $-23_{-4}^{+5}$  and  $41_{-9}^{+12}$  s, respectively.

We have divided the profile into three phases, namely, the “pre-shot” phase, the “peak” phase, and the “decay” phase, and made a spectrum from each phase. We have subtracted the pre-shot spectrum from each of the peak and the decay spectra to extract the pure shot component. The pure shot component is shown in Fig. 5, together with the pre-shot spectrum. The 3-20 keV fluxes in the peak and decay phases are  $1.9 \times 10^{-10}$  erg  $\text{s}^{-1}$   $\text{cm}^{-2}$  and  $5.7 \times 10^{-11}$  erg  $\text{s}^{-1}$   $\text{cm}^{-2}$ , respectively. The shot component is well fit by either an absorbed power-law model or an absorbed thermal bremsstrahlung model. No emission line is detected. The total spectrum integrated over all data taken on MJD =

52235 is expressed as an attenuated bremsstrahlung model and require the addition of a broad iron line of  $7.00 \pm 0.02$  keV. The hydrogen column density decreases in the decay phase from  $60_{-32}^{+50} \times 10^{22}$  cm $^{-2}$  to  $18_{-13}^{+20} \times 10^{22}$  cm $^{-2}$  in both models used to fit the data. The best fit thermal bremsstrahlung temperature and power-law photon index at the peak are  $kT_1 = 14_{-9}^{+86}$  keV and  $1.6_{-0.3}^{+0.3}$ , respectively. The index or the temperature do not change significantly during the decay. The unabsorbed 2-10 keV luminosity at the peak are fitted to be  $L_1 = 4.7_{-1.9}^{+1.5} \times 10^{35}$  erg s $^{-1}$  assuming a distance of  $D = 4.85$  kpc (Vermeulen et al. 1993).

**Interpretation** This is the first detection of a rapid X-ray variability with a time scale less than 300 s from SS 433 (Kotani et al. 2002, 2003; Safi-Harb & Kotani 2003). Although this source had been observed for numerous times with various X-ray observatories, only variability with time scales as long as or longer than a day had been reported. For example, Einstein observed the source to vary by a factor of 2 on time scales of a day (Band 1989), and daily variations other than the orbital and precessional modulations are seen in Ginga and ASCA data (Yuan et al. 1995; Kotani 1997). Temporal analysis of ROSAT data shows flickering around 3-10 s, but this variability does not appear consistently (Safi-Harb 1997). Since the detection with RXTE in 2001 (Kotani et al. 2002, 2003; Safi-Harb & Kotani 2003), evidences of rapid X-ray variability have been accumulated. Chakrabarti et al. (2003) report on X-ray variability with time scales of a few minutes detected in 2002 with RXTE, and Revnivtsev et al. (2004) detected a significant X-ray variability with time scales as short as 100 s with RXTE in 2004.

The absence or weakness of a rapid X-ray variability had been explained in terms of the X-ray-emitting jet as long as or longer than  $10^{12}$  cm. Together with the QPO-like feature in the power density spectrum, this shot-like variability implies the presence of X-ray sources smaller than  $10^{12}$  cm in the system. Considering that these shots coincide a massive jet ejection event, we further assume that they are related to the ejection in the following discussion.

Since the spectral fit is consistent with a decrease of the absorption hydrogen column density during the evolution of the shots, we attribute the rise of the shots to the decrease of attenuating matter, or in other words, the emergence of an X-ray-emitting small plasma bullet from behind attenuating matter. Each shot literally corresponds to a shot of a small plasma bullet from the nozzle. This interpretation is different from that of the X-ray variability seen in GRS 1915+105, which is explained in terms of the rapid removal and replenishment of matter forming the inner part of an accretion disk (Belloni et al. 1997). Since both thermal and non-thermal spectral models are consistent with the observed spectrum, it is difficult to determine the emission mechanism. But in either case, physical quantities

of the emitting bullets would be derived as follows.

**Thin-thermal emission** Given a spherical, thin-thermal, freely expanding plasma bullet with a temperature  $T(t)$ , a radius  $R(t) = v_{\text{exp}}t$ , an expanding velocity  $v_{\text{exp}} = \text{const.}$ , and a total number of electrons  $N_e = \text{const.}$ , the cooling would be governed with the equation

$$\frac{3}{2}(1+X)N_e k_B \frac{dT}{dt} = -\frac{\Lambda(T)XN_e^2}{\frac{4}{3}\pi R^3} - 3(\gamma-1)\frac{3}{2}(1+X)N_e k_B \frac{Tv_{\text{exp}}}{R}, \quad (3)$$

where  $X = N_i/N_e$  is the ratio of the total number of ions to that of electrons assumed to be 0.93117,  $k_B$  is the Boltzmann constant, and  $\gamma$  is the adiabatic index, assumed to be 5/3. The first term on the right-hand side corresponds to radiative cooling, and the coefficient  $\Lambda(T)$  is defined so that  $\Lambda(T)N_e/(4\pi R^3/3)N_i/(4\pi R^3/3)$  equals to the emitted power per unit volume. The last term corresponds to expansion: For expanding plasma with a volume  $V(t)$ ,

$$V^{\gamma-1}dT = -T(\gamma-1)V^{\gamma-2}dV \quad (4)$$

is derived from the relation  $TV^{\gamma-1} = \text{constant}$ . Substituting  $V = 4\pi R^3/3$  to Eq. (4), the cooling rate by expansion,  $dT/dt = -3(\gamma-1)Tv_{\text{exp}}/R$  is obtained, which is equivalent to the last term of Eq. (3). The time parameter  $t$  is defined so that  $t = 0$  at  $R = 0$ , although the radius can never be zero. If the coefficient  $\Lambda(T)$  is proportional to  $\sqrt{T}$  and written in the form  $\Lambda(T) = \Lambda_T\sqrt{T}$ , Eq. (3) has an analytic solution

$$\begin{aligned} \sqrt{T} &= \left( \sqrt{T_1} - \frac{\Lambda_T N_e X}{4\pi(\frac{7}{2} - \frac{3}{2}\gamma)(1+X)k_B v_{\text{exp}} R_1^2} \right) \left( \frac{R}{R_1} \right)^{-\frac{3}{2}\gamma + \frac{3}{2}} \\ &\quad + \frac{\Lambda_T X N_e}{4\pi(\frac{7}{2} - \frac{3}{2}\gamma)(1+X)k_B v_{\text{exp}} R_1^2} \left( \frac{R}{R_1} \right)^{-2} \\ &= \sqrt{T_1} \left[ \left( 1 - \frac{L_1 \tau_{\text{exp}}}{2E_1} \right) \left( \frac{R}{R_1} \right)^{-1} + \frac{L_1 \tau_{\text{exp}}}{2E_1} \left( \frac{R}{R_1} \right)^{-2} \right], \end{aligned} \quad (5)$$

$$E_1 = \frac{3}{2}(1+X)N_e k_B T_1 \quad (6)$$

$$L_1 = \frac{3\Lambda_T \sqrt{T_1} X N_e^2}{4\pi R_1^3} \quad (7)$$

$$\tau_{\text{exp}} = R_1/v_{\text{exp}} \quad (8)$$

where the subscript “1” denotes the value at the peak.  $E_1$ ,  $L_1$ , and  $\tau_{\text{exp}}$  correspond to the thermal energy, the luminosity of the bullet at the peak, and the time scale of expansion, respectively. The ratio  $L_1\tau_{\text{exp}}/(2E_1)$  represents the fraction of the thermal energy in the

bullet lost by radiation (cf. Kotani et al. 1996). Using Eq. (5), the luminosity of the bullet can be written as

$$L = L_1 \left[ \left( 1 - \frac{L_1 \tau_{\text{exp}}}{2E_1} \right) \left( \frac{R}{R_1} \right)^{-4} + \frac{L_1 \tau_{\text{exp}}}{2E_1} \left( \frac{R}{R_1} \right)^{-5} \right]. \quad (9)$$

The expansion velocity  $v_{\text{exp}}$  is estimated from the observed temperature as  $v_{\text{exp}} = \sqrt{k_B T_1 / (\mu m_H)} = 1.5_{-0.6}^{+2.5} \times 10^8 \text{ cm s}^{-1}$ , where  $m_H$  is the mass of a hydrogen atom and  $\mu$  is the mean molecular weight assumed to be 0.587922. In 40 s, the luminosity of the plasma decreases by a factor of  $1/e$ . Substituting the factor into Eq. (9), we obtain

$$\frac{L_2}{L_1} = \frac{1}{e} = \left( 1 - \frac{L_1 \tau_{\text{exp}}}{2E_1} \right) \left( \frac{R_2}{R_1} \right)^{-4} + \frac{L_1 \tau_{\text{exp}}}{2E_1} \left( \frac{R_2}{R_1} \right)^{-5}, \quad (10)$$

where the subscript “2” denotes the value at the decay phase. Because the ratio of the radiation loss to the internal energy  $L_1 \tau_{\text{exp}} / (2E_1)$  is between 0 and 1, the expansion in 40 s is constrained as  $\exp[1/5] < R_2/R_1 < \exp[1/4]$  from the above equation. Substituting  $R_2 = R_1 + v_{\text{exp}} \times 40 \text{ s}$ , we obtain the radius as  $R_1 = 2.2_{-0.9}^{+3.6} \times 10^{10} \text{ cm}$ . From this radius and an observed quantity  $L_1$ , all other parameters are derived;  $1.06 \times 10^2 < \tau_{\text{exp}} < 1.35 \times 10^2 \text{ s}$ , the number of electrons  $N_e = 1.0_{-0.5}^{+2.1} \times 10^{45}$ , the number density of electrons  $n_{e1} = 4.1_{-3.7}^{+9.2} \times 10^{13} \text{ cm}^{-3}$ , and the thermal energy  $E_1 = 0.7_{-0.6}^{+13.7} \times 10^{38} \text{ erg}$ . Assuming that the bullet is moving at 0.26 c, the kinetic energy of the bullet is estimated to be  $0.6_{-0.3}^{+1.2} \times 10^{41} \text{ erg}$ . The assumption is consistent with the observed rise time of 20 s, which is naturally explained by the time in which a bullet appears from a nozzle. Eq. (5) is written with these estimates as

$$\sqrt{T} = \sqrt{14 \text{ [keV]}} \left[ 0.3 \left( \frac{R}{1.6 \times 10^{10} \text{ [cm]}} \right)^{-1} + 0.7 \left( \frac{R}{1.6 \times 10^{10} \text{ [cm]}} \right)^{-2} \right], \quad (11)$$

where errors are omitted.

Since a shot and the unmodulated component coexist, the bullets and the continuously emanating jet may coexist. In that case, the small plasma bullets can be interpreted as bright knots in the continuous jet. The knots are created when the mass outflow rate or the density of the continuous jet is temporarily increased. A temporal increase of temperature is not plausible, because it would result in a change of the spectrum, which has not been observed. The properties of the knots would not be much different from those of the small plasma bullets discussed above, and the estimates above are valid if the knots or bullets coexist with the continuous jet.

**Synchrotron emission** Because the spectral shape does not much change in the decay and because no iron line is detected in the shot component, a non-thermal emission from



expanding bullets also can account for the shot component. As for the steady non-variable component, it is definitely a thin-thermal emission with Doppler-shifted iron lines. Therefore, it is natural to interpret the shot component as a thermal emission, and an interpretation of non-thermal emission is rather eccentric. In the following paragraph, we show physical parameters of a plasma bullet assuming that the bullets emit X ray via synchrotron radiation.

A power-law distribution of synchrotron electrons,

$$f(\gamma)d\gamma \equiv \begin{cases} \frac{-p+1}{\gamma_{\max}^{-p+1}-1}n_{e,\text{syn}}\gamma^{-p}d\gamma \approx (p-1)n_e\gamma^{-p}d\gamma & (1 < \gamma \leq \gamma_{\max}) \\ 0 & (\gamma_{\max} < \gamma) \end{cases} \quad (12)$$

is assumed, where  $\gamma$  is Lorentz factor of electrons,  $n_{e,\text{syn}}$  is the synchrotron-electron number density, and  $p = 2.2_{-1.0}^{+1.4}$  is the electron energy index derived from the photon index  $\Gamma = (p + 1)/2$ . The maximum Lorentz factor should be at least  $\gamma_{\max} > 1.4 \times 10^5$  to account for the X-ray emission up to 10 keV. Optically thin synchrotron flux from such a sphere is expressed as

$$F_\nu = \frac{\chi(p)}{4\pi}n_{e,\text{syn}}\frac{e^3}{mc^2}B^{p/2+1/2}\left(\frac{4\pi mc\nu}{3e}\right)^{-p/2+1/2}\frac{4\pi R^3/3}{D^2} \quad (13)$$

$$\chi(p) \equiv \frac{3^{1/2}2^{p/2-1/2}(p-1)\Gamma\left(\frac{p}{4}+\frac{19}{12}\right)\Gamma\left(\frac{p}{4}-\frac{1}{12}\right)\Gamma\left(\frac{p}{4}+\frac{5}{4}\right)}{(p+1)\Gamma\left(\frac{p}{4}+\frac{7}{4}\right)} \quad (14)$$

where  $\nu$  is frequency, and  $B$  is the magnetic field strength in the plasma, (e.g., Hjellming & Han (1995)). By substituting the observed flux  $F_\nu(1 \text{ keV}) = 1.0_{-0.5}^{+1.0} \times 10^{-2} \text{ photons cm}^{-2} \text{ s}^{-1} \text{ keV}^{-1}$  into Eq. (13), the magnetic field strength  $B$  and the total number of electrons in a bullet  $N_e$  are constrained as

$$\log_{10} [N_e B^{p/2+1/2} [\text{G}]] = 44.6_{-2.9}^{+3.0}, \quad (15)$$

where the rather large uncertainty is due to the uncertainty of the electron energy index  $p$ .

As the bullet expands, each high-energy electron loses energy as  $E = (R/R_1)^{-1}$  and the magnetic field and the luminosity decreases as  $B = B_1 \times (R/R_1)^{-2}$  and  $L = L_1(R/R_1)^{-2p}$ , respectively. Radiative cooling and heating are neglected. Thus a decrease of flux by a factor of  $1/e$  corresponds to an adiabatic expansion by  $1.26_{-0.10}^{+0.25}$  of the radiating bullet. Further assuming that the bullet is proceeding at  $0.26 c$  with an expanding half angle of  $2.1^\circ$ , which are the same value as the velocity and the half opening angle of the continuous jet (Namiki et al. 2003), the expansion velocity is estimated as  $v_{\text{exp}} = 2.9 \times 10^8 \text{ cm s}^{-1}$ . From this expansion velocity and the expansion factor obtained above, the radius of the plasma is determined as  $R = 4.5_{-1.4}^{+1.4} \times 10^{10} \text{ cm}$ , which is consistent with the rise time of 20 s.

The synchrotron-electron number density and the strength of the magnetic field can be estimated if their energies are assumed to be in equipartition, i.e.,

$$\frac{B^2}{8\pi} = \int_1^{\gamma_{\max}} \frac{p-1}{\gamma_{\max}^{-p+1} - 1} n_e mc^2 \gamma^{-p+1} d\gamma \quad (16)$$

$$\approx \begin{cases} \frac{p-1}{-p+2} \gamma_{\max}^{-p+2} n_e mc^2 & (1 < p < 2) \\ \frac{p-1}{p-2} n_e mc^2 & (2 < p). \end{cases} \quad (17)$$

Substituting an electron energy index of  $p = 2.2$ , we obtain  $B = 1.8 \times 10^2$  G and  $n_e = 2.4 \times 10^8$  cm<sup>-3</sup>. The total number of electrons and internal energy in a bullet are estimated as  $N_e = 9 \times 10^{40}$  per shot and  $E_{\text{syn}} = 5.3 \times 10^{35}$  erg, respectively. These number of electrons and internal energy derived here are smaller by orders of magnitude than those of the thin-thermal case.

**Comptonized emission** If the emission mechanism is inverse-Compton scattering of optical photons, the seed-photon density would decrease and the emission would decay as the plasma bullet gets away from the central engine. Based on this Comptonized-emission model, the parameters of the plasma bullet, such as the electron number density, the total number of electrons, and the total energy of electrons, are estimated. They are found to be not much different from those in the case of synchrotron emission, although the uncertainties of parameters are larger in the case of inverse-Comptonization.

### 3.4. The massive jet

Based on the bullets model, we suggest an explanation of the massive jet ejection: During the massive jet ejection event, small discrete plasma bullets, or knots in the continuously emanating flow, are successively ejected at random intervals of  $\sim 150$  s. The radius of bullets is estimated as  $R_1 = 2.2_{-0.9}^{+3.6} \times 10^{10}$  cm. The X-ray emission from the small plasma bullets, either thermal or non-thermal, decays in 40 s as it expands. Assuming that the most active state lasts 3 days, the total number of small bullets ejected in a single massive jet event is estimated to be 1700. The total mass and total kinetic energy of all the 1700 bullets are  $3.3_{-1.8}^{+6.7} \times 10^{24}$  g and  $1.0_{-0.5}^{+2.1} \times 10^{44}$  erg, respectively. The average mass ejection rate and average kinetic luminosity over 3 days are  $0.7_{-0.4}^{+1.6} \times 10^{16}$  g s<sup>-1</sup> and  $3.9_{-2.1}^{+8.0} \times 10^{38}$  erg s<sup>-1</sup>, respectively. In the case of synchrotron emission from baryonic plasma, only the lower limits of mass and kinetic energy are derived; the total mass and total kinetic energy of the 1700 bullets would be at least  $3.0 \times 10^{20}$  g and  $9.1 \times 10^{39}$  erg, respectively, and the average mass ejection rate and average kinetic luminosity would be at least  $1.1 \times 10^{15}$  g and  $3.5 \times 10^{34}$  erg s<sup>-1</sup>, respectively.

The estimated average kinetic luminosity of  $\sim 10^{38}$  erg s $^{-1}$  is considerably lower than estimates based on the quiescent or normal state. For example, Kotani (1997) has calculated the kinetic luminosity as  $1 \times 10^{40}$  erg s $^{-1}$  based on ASCA data, Marshall et al. (2002) as  $3.2 \times 10^{38}$  erg s $^{-1}$  based on HETGS/Chandra data, and Brinkmann et al. (2005) as  $5 \times 10^{39}$  erg s $^{-1}$  based on EPIC/XMM-Newton data. It is puzzling that the mass outflow rate and kinetic luminosity in the massive jet ejection are not so “massive” compared to those of the steady continuous jet flow seen in most occasions. There are several possibilities to account for the inconsistency in terms of the bullets model: 1) The mass outflow rate and kinetic luminosity of a massive jet are not larger than those of quiescent steady jet, but the efficiency to accelerate electrons contributing to synchrotron radio emission is far larger. 2) The massive jet is not an assembly of the small plasma bullets, but mainly supplied with the steady flow which coexists with the bullets. 3) In spite of the monitoring observation with a sampling rate of 3 ks a day, we have missed the moment of the true massive jet ejection, which lasts only, say, hours, and a massive jet of  $10^{44} - 10^{45}$  erg is ejected at a maximum outflow rate of  $10^{40} - 10^{41}$  erg s $^{-1}$ . We do not yet have an evidence supporting one of them, but suggest that the second case is unlikely, in which the unvariable X-ray component is expected to rise as the radio flux densities rise.

Another question is whether X-ray variability is really related to radio flaring, which is associated with blob rebrightening events out of the system core. At 1.6 GHz, radio flares peak at 35 AU from the core (Paragi et al. 1999). If radio flares were caused by an environmental condition, it would not be detectable in X-ray band at the ejection, and the coincidence of the rapid X-ray variability and the massive jet event would be accidental. However, Paragi et al. (1999) suggest that the rebrightening is due to the attenuation by outflowing gas around the core. If the cause of radio flares is not an environmental condition but a core activity, the activity which changes the radio flux by a factor of 2 might be detectable in X-ray band. That should be tested in future multi-wavelength observations.

X-ray shots are firstly seen in the data from MJD = 52225, a week before its maximum activity and the onset of a second radio flare. Provided that shots precede a radio flare, we can predict a massive jet-ejection event based on X-ray monitoring data. On detection of X-ray shots, notice of a massive jet ejection to occur in a week can be sent to ground and space observatories. An observation campaign covering a massive jet ejection is possible. There is still a possibility that the duration of a massive jet ejection is shorter than 1 day and the moment has been missed even in our observations. It can be confirmed in future observations. And this technique may be applicable for prediction of massive jet ejections from other microquasars. In spite of numerous observations performed so far, it is not yet known whether massive jet ejections from other microquasars such as GRS 1915+105 are also preceded by a precursor or not. As a specially coordinated observation is required to

detect the shot-like variability from SS 433, a carefully coordinated observations plan is desirable to observe GRS 1915+105 in a massive jet ejection event with an X-ray mission. The findings reported here imply that new and important physics of a microquasar is revealed by observing massive jet ejections. The observation of these events is essential to explore the nature of microquasars. Therefore the technique to observe massive jet ejections is one of the most important results from this study. Future observations of massive jet ejections from microquasars are encouraged.

T. K. is supported by a 21st Century COE Program at Tokyo Tech “Nanometer-Scale Quantum Physics” by the Ministry of Education, Culture, Sports, Science and Technology. S. A. T. is very grateful to the Russian Base Researches Foundation for support of the SS 433 monitoring with the RATAN-600 radio telescope. K. K. is supported by a grant-in aid 16740121 from the Ministry of Education, Culture, Sports, Science and Technology of Japan. We thank the anonymous referee for useful comments and suggestions to improve this paper.

## REFERENCES

- Band, D. 1989, *ApJ*, 336, 937
- Belloni, T., Mendez, M., King, A. R., van der Klis, M., & van Paradijs, J. 1997, *ApJ*, 479, L145
- Brinkmann, W., Kotani, T., & Kawai, N. 2005, *A&A*, 431, 575
- Chakrabarti, S. K., Pal, S., Nandi, A., Anandarao, B. G., & Mondal, S. 2003, *ApJ*, 595, L45
- Fender, R. P. 2001, in *Proc. ESO Workshop: Black holes in binaries and galactic nuclei*, ed. L. Kaper, E. P. J. van den Heuvel, & Woudt, P. A. (Berlin: Springer-Verlag), 193
- Fiedler, R. L., et al. 1987, *AJ*, 94, 1244
- Foster, R. S., et al. 1996, *ApJ*, 467, L81
- Gies, D. R., McSwain, M. V., Riddle, R. L., Wang, Z., Wiita, P. J., & Wingert, D. W. 2002, *ApJ*, 566, 1069
- Goranskii, V. P., Esipov, V. F., & Cherepashchuk, A. M. 1998, *Astron. Reports*, 42, 209
- Hasegawa, T., Malasan, H. L., Kawakita, H., Obayashi, H., Kurabayashi, T., Nakai, T., Hyakkai, M., & Arimoto, N. 2004, *PASJ*, 56, 295

- Hjellming, R. M., & Han, X. 1995, in *X-Ray Binaries*, ed. W. H. G. Lewin, J. van Paradijs, & E. P. J. van den Heuvel (Cambridge: Cambridge University Press), 308
- Kawai, N. 1989, in *Proc. 23rd ESLAB Symp. on Two-topic in X-Ray Astronomy*, (European Space Agency, Noordwijk), 453
- Kinugasa, K., et al. 2002, *ApJ*, 577, L97
- Klein-Wolt, M., Fender, R. P., Pooley, G. G., Belloni, T., Migliari, S., Morgan, E. H., & van der Klis, M. 2002, *MNRAS*, 331, 745
- Korolkov, D. V., & Pariiskii, I. N. 1979, *S&T*, 57, 324
- Kotani, T., Kawai, N., Matsuoka, M., & Brinkmann, W. 1996, *PASJ*, 48, 619
- Kotani, T. 1997, *Doctoral Thesis*, University of Tokyo
- Kotani, T., & Trushkin, S. 2001, *IAU Circ.*, 7747
- Kotani, T., Band, D., Denissyuk, E. K., Kawai, N., Kinugasa, K., Namiki, M., Safi-Harb, S., & Trushkin, S. 2002, *ASP Conf. Ser. 279: Exotic Stars as Challenges to Evolution*, 279, 19
- Kotani, T., Trushkin, S., Denissyuk, E. K., Kawakita, N., Kinugasa, K., Safi-Harb, S., & Band, D. 2003, in *New Views on Microquasars*, ed. P. Durouchoux, Y. Fuchs, & J. Rodriguez (Kolkata: Centre for Space Physics), 265
- Marshall, H. L., Canizares, C. R., & Schulz, N. S. 2002, *ApJ*, 564, 941
- Mirabel, I. F., Dhawan, V., Chaty, S., Rodriguez, L. F., Marti, J., Robinson, C. R., Swank, J., & Geballe, T. 1998, *A&A*, 330, L9
- Mirabel, I. F., & Rodríguez, L. F. 1994, *Nature*, 371, 46
- Mirabel, I. F., & Rodríguez, L. F. 1999, *ARA&A*, 37, 409
- Mironov, A. V., & Tereshchenko, V. M. 1998, *Baltic Astron.*, 7, 351
- Muno, M. P., Remillard, R. A., Morgan, E. H., Waltman, E. B., Dhawan, V., Hjellming, R. M., & Pooley, G. 2001, *ApJ*, 556, 515
- Namiki, M., Kawai, N., & Kotani, T. 2001, *ASP Conf. Ser. 251: New Century of X-ray Astronomy*, 251, 390
- Namiki, M., Kawai, N., Kotani, T., & Makishima, K. 2003, *PASJ*, 55, 281

- Paragi, Z., Vermeulen, R. C., Fejes, I., Schilizzi, R. T., Spencer, R. E., & Stirling, A. M. 1999, *A&A*, 348, 910
- Revnivtsev, M., et al. 2004, *A&A*, 424, L5
- Rupen, M. P., Hjellming, R. M., & Mioduszewski, A. J. 1998, *IAU Circ.*, 6938
- Safi-Harb, S. 1997, Ph.D. Thesis, University of Wisconsin.
- Safi-Harb, S., & Kotani, T. 2003, in *New Views on Microquasars*, ed. P. Durouchoux, Y. Fuchs, & J. Rodriguez (Kolkata: Centre for Space Physics), 279
- Trushkin, S. A., Bursov, N. N., & Nizhelskij, N. A. 2003, *Bull. Spec. Astrophys. Obs.*, 56, 57
- Ueda, Y., et al. 2002, *ApJ*, 571, 918
- Vermeulen, R. C., Schilizzi, R. T., Spencer, R. E., Romney, J. D., & Fejes, I. 1993, *A&A*, 270, 177
- Watson, M. G., Willingale, R., Grindlay, J. E., & Seward, F. D. 1983, *ApJ*, 273, 688
- Yuan, W., Kawai, N., Brinkmann, W., & Matsuoka, M. 1995, *A&A*, 297, 451

Table 1: Observation log

Start (MJD)	End (MJD)	Exposure Time (ks)	PCU <sup>a</sup>
2001/11/09 07:10 (52222.299)	2001/11/09 08:11 (52222.341)	3.6	0234
2001/11/10 05:19 (52223.222)	2001/11/10 06:21 (52223.265)	3.7	0234
2001/11/11 06:47 (52224.283)	2001/11/11 07:47 (52224.325)	3.6	0234
2001/11/12 06:35 (52225.275)	2001/11/12 07:35 (52225.316)	3.5	0234
2001/11/13 04:46 (52226.199)	2001/11/13 05:46 (52226.240)	3.5	0234
2001/11/14 06:11 (52227.258)	2001/11/14 07:13 (52227.301)	3.7	0234
2001/11/15 06:00 (52228.250)	2001/11/15 07:01 (52228.293)	3.7	0234
2001/11/16 07:26 (52229.310)	2001/11/16 08:32 (52229.356)	4.0	023
2001/11/17 07:14 (52230.302)	2001/11/17 08:20 (52230.349)	4.1	023
2001/11/19 03:41 (52232.154)	2001/11/19 04:33 (52232.190)	3.1	0234
2001/11/20 06:40 (52233.278)	2001/11/20 07:46 (52233.324)	4.0	02
2001/11/21 08:05 (52234.337)	2001/11/21 09:16 (52234.387)	4.3	023
2001/11/22 07:54 (52235.330)	2001/11/22 09:05 (52235.379)	4.2	024
2001/11/23 04:32 (52236.189)	2001/11/23 05:29 (52236.229)	3.5	024
2001/11/24 01:11 (52237.050)	2001/11/24 01:54 (52237.080)	2.6	02
2001/11/25 05:45 (52238.240)	2001/11/25 06:47 (52238.283)	3.7	012

<sup>a</sup> Proportional counter units in operation.

Table 2: Spectral parameters

Start (MJD)	$kT$ (keV)	$E_N$ (keV)	$F_N$ (ph s <sup>-1</sup> cm <sup>-2</sup> )	$E_B$ (keV)	$\sigma_B$ (keV)	$F_B$ (ph s <sup>-1</sup> cm <sup>-2</sup> )	$\chi^2/\text{d.o.f.}$
52222.299	35	6.5	$5.1 \times 10^{-4}$	6.92	0.83	$2.2 \times 10^{-3}$	30.5/31
52223.222	49	6.4	$4.7 \times 10^{-4}$	6.98	0.81	$2.2 \times 10^{-3}$	51.5/31
52224.283	47	6.5	$4.7 \times 10^{-4}$	6.98	0.83	$2.2 \times 10^{-3}$	29.7/31
52225.275	56	6.7	$5.2 \times 10^{-4}$	6.95	1.00	$2.9 \times 10^{-3}$	57.0/31
52226.199	55	6.8	$6.5 \times 10^{-4}$	6.90	1.07	$3.1 \times 10^{-3}$	82.8/31
52227.258	45	6.9	$5.5 \times 10^{-4}$	6.90	1.10	$3.1 \times 10^{-3}$	45.0/31
52228.250	37	6.8	$4.8 \times 10^{-4}$	6.92	0.99	$2.8 \times 10^{-3}$	39.9/31
52229.310	48	6.9	$6.3 \times 10^{-4}$	6.94	1.07	$2.9 \times 10^{-3}$	38.7/31
52230.302	37	6.9	$3.4 \times 10^{-4}$	6.97	0.95	$2.3 \times 10^{-3}$	49.6/31
52232.154	38	7.0	$5.9 \times 10^{-4}$	6.88	1.21	$3.3 \times 10^{-3}$	72.2/31
52233.278	25	7.0	$2.2 \times 10^{-4}$	7.06	0.93	$2.0 \times 10^{-3}$	87.1/30
52234.337	21	6.9	$2.2 \times 10^{-4}$	7.11	1.07	$2.1 \times 10^{-3}$	42.1/30
52235.330	48	7.0	$6.0 \times 10^{-4}$	6.88	1.12	$2.5 \times 10^{-3}$	38.4/30
52236.189	53	7.0	$5.1 \times 10^{-4}$	6.92	1.05	$2.7 \times 10^{-3}$	53.1/30
52237.050	55	7.0	$6.6 \times 10^{-4}$	6.74	1.24	$3.0 \times 10^{-3}$	51.9/30
52238.240	42	7.1	$6.9 \times 10^{-4}$	6.92	1.27	$3.4 \times 10^{-3}$	42.9/30

The least significant digit of each best-fit value has an uncertainty of the same order. For 2-10 keV flux, see Fig. 1.



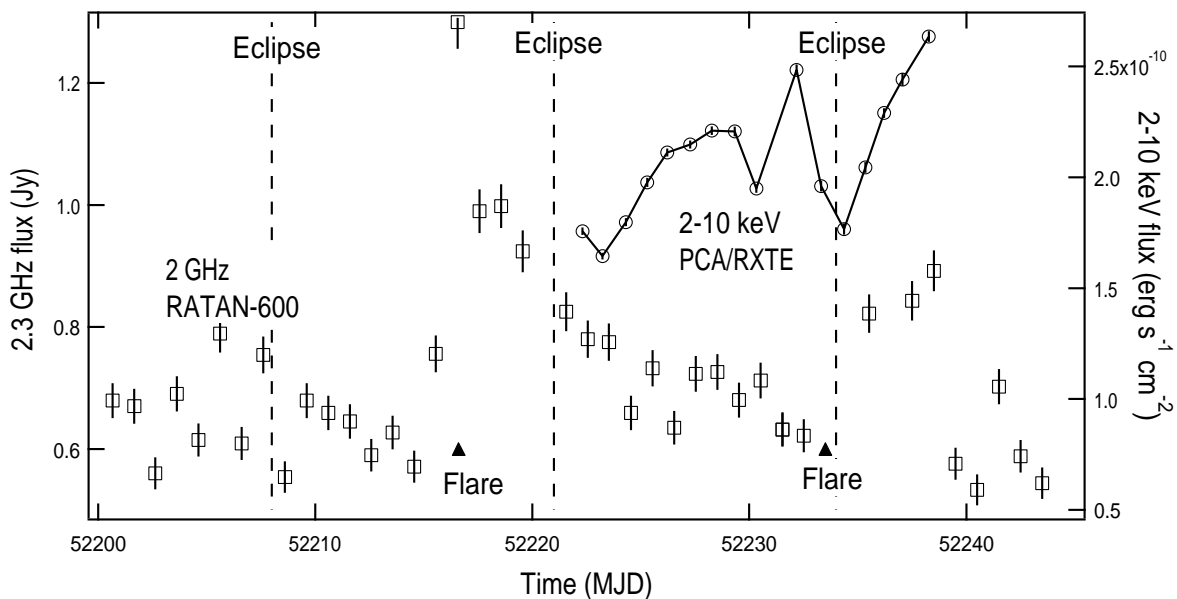


Fig. 1.— 2.3 GHz radio light curve (open squares with error bars) and 2-10 keV X-ray light curve (open circles with error bars and solid line) of SS 433. The radio flux taken with RATAN-600 shows two flares, or massive jet-blob ejections, indicated by filled triangles. The epochs of eclipse are indicated in dashed lines. The first flare has triggered RXTE monitoring observations. The rise of the second flare is not prominent because of a lack of the monitoring data on MJD = 52234 due to bad weather condition. The X-ray fluxes show a peak just before the second radio flare and then a dip coinciding with an eclipse.

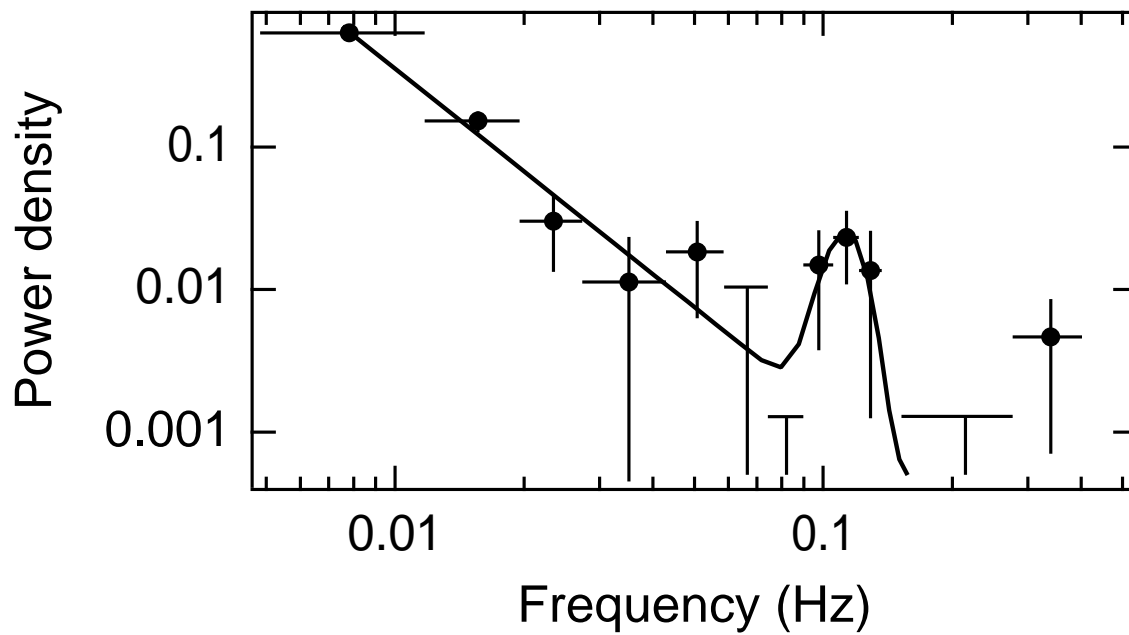


Fig. 2.— Sum of power density spectra of the X-ray data. The sum of all 16 spectra and the best fit model of a power-law model plus a Gaussian (solid line) are plotted. The data points and upper limits are marked as filled circles and T-shaped bars, respectively. A feature which can be interpreted as a QPO centered at  $0.1127 \pm 0.0072$  Hz with a Gaussian sigma of  $0.011 \pm 0.006$  Hz is seen.

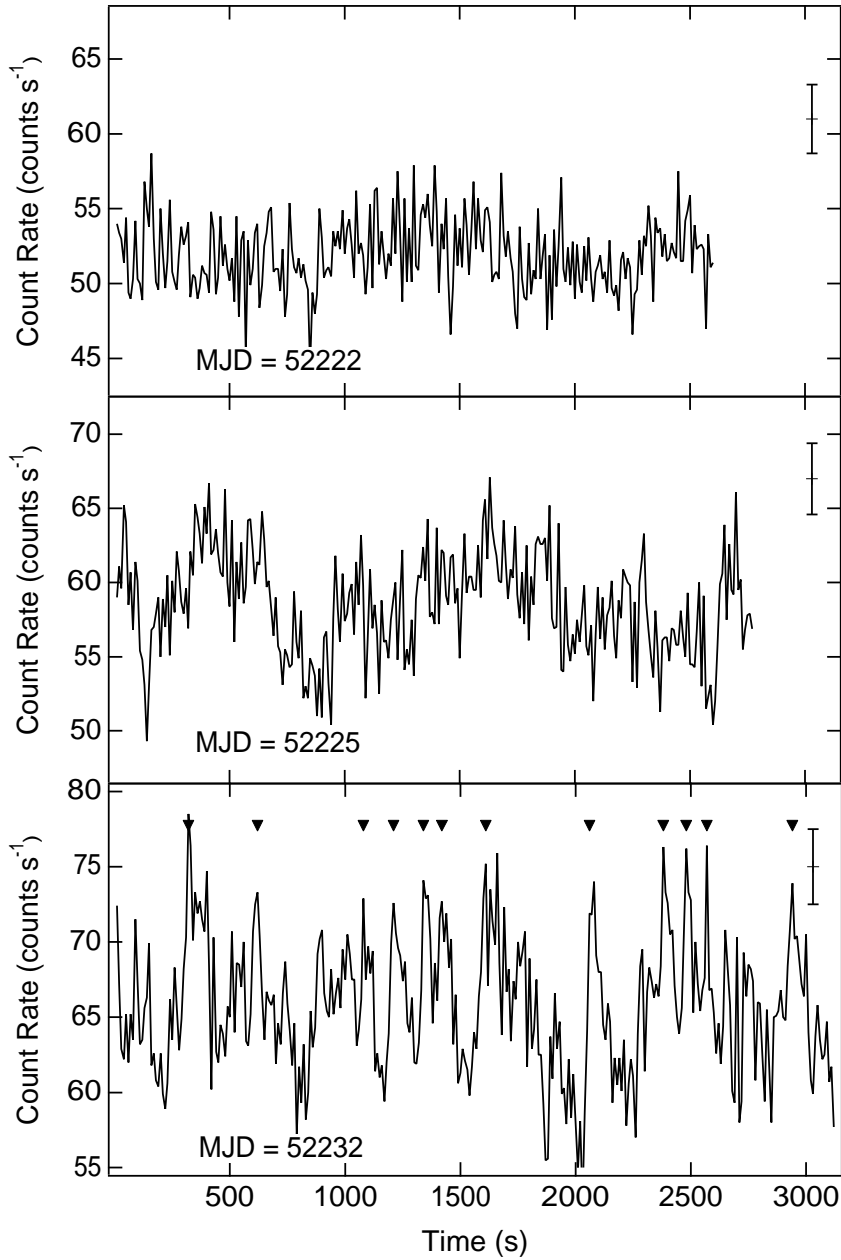


Fig. 3.— Blown-up X-ray light curves taken on MJD = 52222 (upper panel), 52225 (middle), and 52232 (lower). Only the energy band higher than iron and nickel lines (8.38 keV for blue-shifted Ni xxvii  $K\alpha$ ) is shown. Typical  $1\sigma$  errors are plotted as crosses. The amplitude of variations on MJD = 52222, if any, is not larger than the error bar. On MJD = 52225, the variations becomes significant, and the amplitude reaches the maximum on 52232. The variation on MJD = 52232 can be interpreted as a series of “shots” or “spikes.” By picking up local maximums in the light curve above a threshold of  $74\text{ counts s}^{-1}$  after at least 2 successive increasing bins (30 s), twelve shots are sampled as indicated by the filled triangles in the lower panel. The criterion of successive increasing bins is necessary to cut local maximums due to fluctuation. The threshold of  $74\text{ counts s}^{-1}$  ( $13\sigma$ ) is chosen so that most shots are sampled only once. This sampling is not exhaustive and a different set of shots may be selected under another criterion.

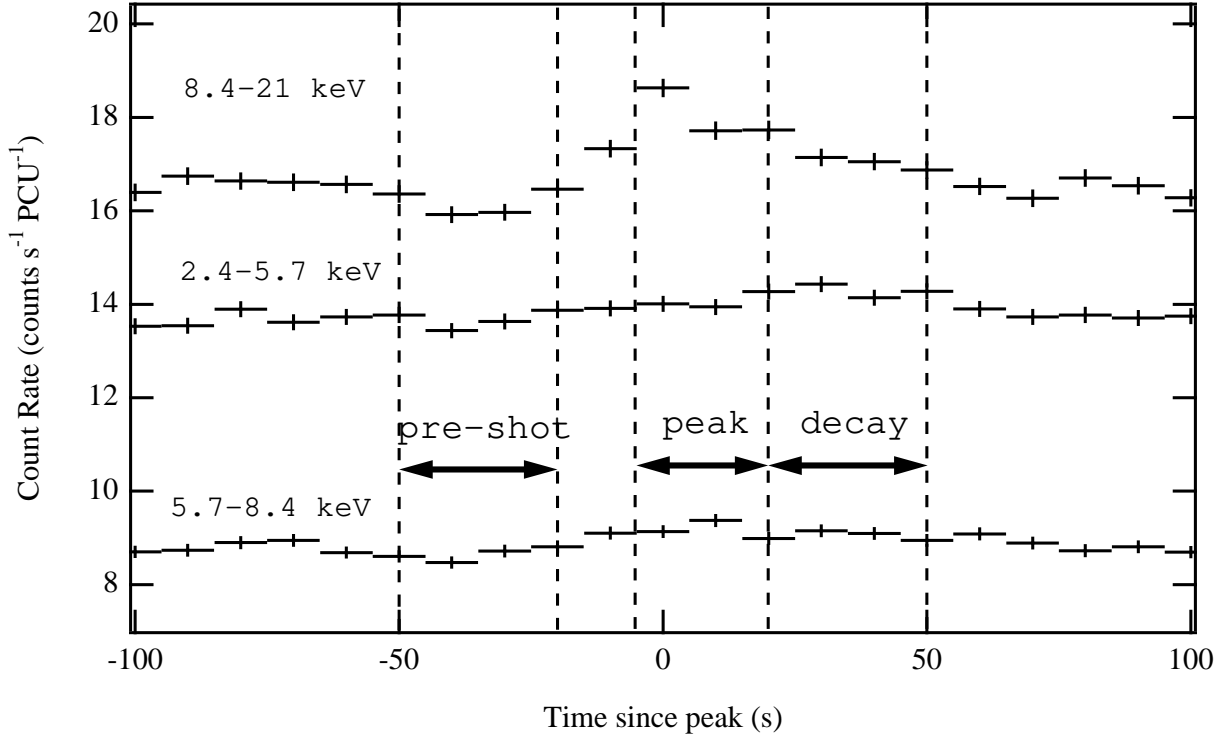


Fig. 4.— Average profile of the twelve shots sampled from the data on MJD = 52232 (Fig. 3). In the 8.4-21 keV band, the shot rises in  $\sim 10$  s and decays slowly ( $\sim 30$  s). In the 2.4-5.7 keV band, the profile is less pronounced: The peak lags behind that in the hard band by  $\sim 30$  s, and both the rise and decay time scales are  $\sim 30$  s. The peak is indistinct in the 5.7-8.4 keV band, too. That implies that the iron-line intensity is not much contributing the shot. For a spectroscopic study, we have divided the profile into three phases; the “pre-shot,” “peak,” and “decay” phases.

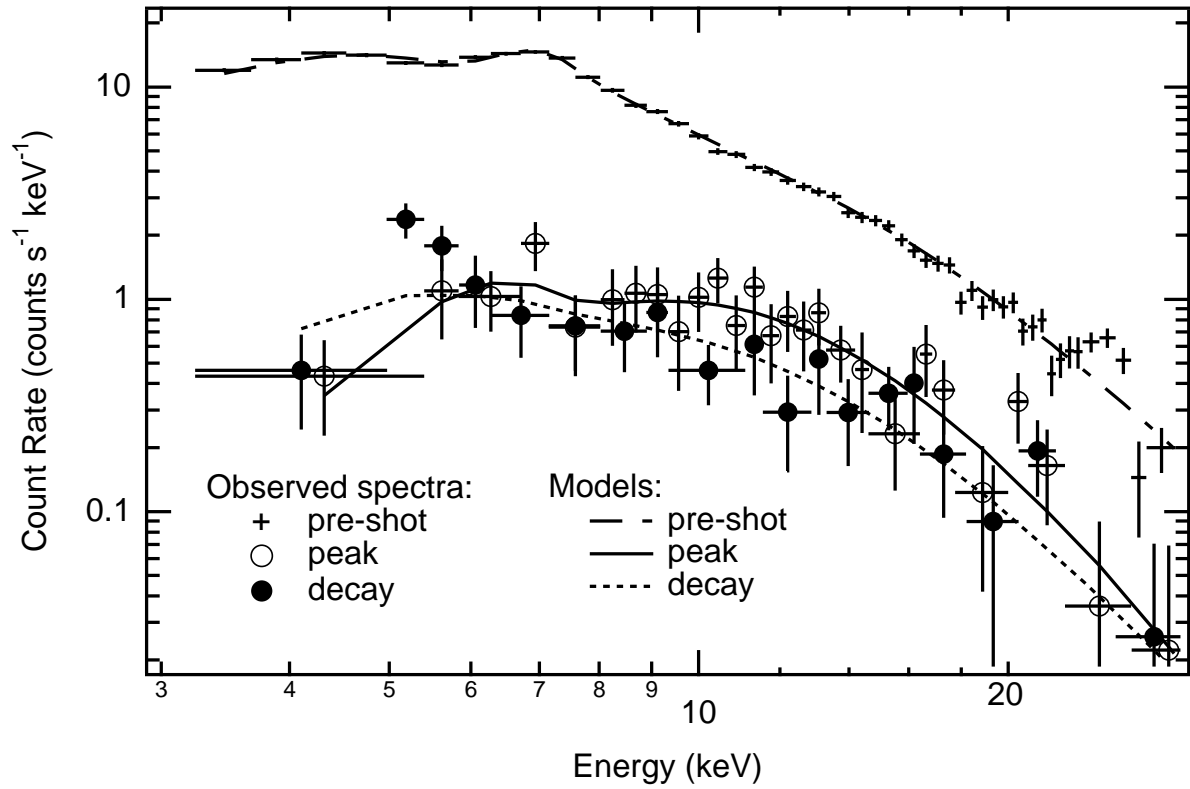


Fig. 5.— Spectra and best-fit models of the pre-shot phase (crosses), the peak phase (open circles), and the decay phase (filled circles). To emphasize the spectral evolution of the shot component, the pre-shot spectrum is subtracted from the peak and decay spectra. The background spectrum made with a tool `pcabackest` is subtracted from the pre-shot spectrum.